Archaeomagnetism in Levant and Mesopotamia reveals the largest changes in the geomagnetic field

Ron Shaar[1], Yves Gallet[2], Yoav Vaknin[1,3], Lilach Gonen[1], Mario A. S. Martin[3], Israel Finkelstein[3,4]

[1]The Institute of Earth Sciences, The Hebrew University of Jerusalem, Jerusalem, 91904, Israel

[2] Université Paris Cité, Institut de Physique du Globe de Paris, CNRS, 75005, Paris, France

[3] Institute of Archaeology of Tel Aviv University, Tel Aviv 6997801, Israel

[3] School of Archaeology and Maritime Cultures, University of Haifa, Haifa, Israel

Corresponding author: Ron Shaar (ron.shaar@mail.huji.ac.il)

Key Points:

- Archaeomagnetic intensity data from 23 groups of pottery collected from 18 consecutive radiocarbon-dated strata in Tel Megiddo (Israel)
- Bayesian radiocarbon-calibrated archaeo-intensity curve of the Levant and Mesopotamia based on stratified mounds and burnt structures
- Four geomagnetic spikes between 1050-600 BCE define new constraints for the maximum intensity and rate of change of the geomagnetic field

Abstract

Our understanding of geomagnetic field intensity prior to the era of direct instrumental measurements relies on paleointensity analysis of rocks and archaeological materials that serve as magnetic recorders. Only in rare cases absolute paleointensity datasets are continuous over millennial timescales, provide sub-centennial resolution, and are directly dated using radiocarbon. As a result, fundamental properties of the geomagnetic field, such as its maximum intensity and maximum rate of change have remained a subject of lively discussion. Here, we place firm constraints on these two quantities using Bayesian modelling of well-dated archaeomagnetic intensity data from the Levant and Upper Mesopotamia. We report new data from 23 groups of pottery collected from 18 consecutive radiocarbon-dated archaeological strata from Tel Megiddo, Israel. In the Near East, the period between 1700-550 BCE is now represented by 87 groups of archaeological artifacts, 57 of which dated using radiocarbon and/or direct association to clear historically-dated events, providing an unprecedented sub-century resolution. Moreover, stratigraphic relation between samples collected from multi-layered sited enable further refinement of the archaeomagnetic ages. The Bayesian curve shows four geomagnetic spikes between 1050 and 600 BCE, with virtual axial dipole moment (VADM) reaching values of 155-162 ZAm^2 – much higher than any prediction from geomagnetic field models. Rates of change associated with the four spikes are ~0.35-0.55 μT/year (~0.7-1.1 ZAm^2/year) – at least twice the maximum rate inferred from direct observations spanning the past 190 years. Moreover, the increase from 1750 BCE to the first spike depicts the Holocene largest change in field intensity.

Plain Language Summary (200 words)

The strength of Earth magnetic field is constantly changing in a chaotic and unpredicted manner. Understanding these changes requires precise information on how the field has changed in the past. Yet, direct instrumental measurements of field intensity began only in the 1840s, offering a merely short time-window. Here, we explore the more ancient field by analyzing a rare collection of radiocarbon-dated archaeological materials from stratified mounds and historically-dated burnt structures in the Levant and Mesopotamia. Based on new data from Tel Megiddo (Armageddon), we construct a continuous curve of geomagnetic field intensity spanning 2500 years, with unprecedented detail and resolution. The curve depicts the evolution of a high-field anomaly, representing the largest change in the geomagnetic field over the Holocene. Between 1750 and 1050 BCE the field rapidly increased toward values of more than twice those of today - much higher than any prediction derived from the available geomagnetic field models. Subsequent oscillations between 1050 and 550 BCE, with extreme peaks namely ‘geomagnetic spikes’, reveal rates of change that are at least twice faster than the fastest change observed since the advent of direct measurements. This is an exemplary case-study where archaeology provides crucial constraints on the geomagnetic field behavior.

1 Introduction

The absolute intensity of the geomagnetic field was first measured by Carl Friedrich Gauss in 1832 (Courtillot & Le Mouel, 2007). Subsequent measurements, with improved precision and spatial resolution, have provided quantitative estimates of the amplitude and rate of geomagnetic field intensity changes, but only at a limited time interval of less than two centuries. Information from periods preceding observational measurements, fundamental for understanding field behavior, is derived from ancient materials that acquired thermoremanent magnetization on cooling from high temperatures. For the past several millennia, archaeological materials are the ultimate source of information (Arneitz et al., 2017; Brown et al., 2021), providing most of the data for late Holocene geomagnetic models (Arneitz et al., 2019; Campuzano et al., 2019; Constable et al., 2016; Nilsson et al., 2014; Panovska et al., 2019; Pavon-Carrasco et al., 2014). Yet, owing to limited precision and accuracy of the dating in the published archaeomagnetic data, geomagnetic stacks, compilations and models are inherently scattered and smoothed, hampering our ability to put firm constraints on geomagnetic field changes. Only ~12% of the published data are directly dated with radiocarbon and in many cases the exact nature and context of the dated material are not documented. Instead, most majority of the available archaeomagnetic ages are based on correlation to regional archaeological chronologies, which can be debated, controversial, and poorly tied to absolute ages (Shaar et al., 2020). Furthermore, unlike reconstructions of the paleomagnetic field direction, which use stratigraphic constraints in sedimentary sequences to obtain continuous time-series, archaeomagnetic intensity datasets are mostly sporadic in time and space. Given the overall uncertainties in the available paleomagnetic and archaeomagnetic data, some the most fundamental properties of the geomagnetic field, such as its maximum intensity and maximum possible rate of change have remained elusive and a subject of a lively and fruitful debate (Davies & Constable, 2018; Korte & Constable, 2018; Livermore et al., 2014; Livermore et al., 2021).

One way to improve the resolution of archaeomagnetic data is focusing efforts on large multi-layered sites, which are assembled from distinct consecutive strata, and can provide data in a stratigraphic order. Few examples for this approach in archaeomagnetism are the datasets from Mari, Tell Atij and Tell Gudeda in Upper Mesopotamia (Gallet & Butterlin, 2015; Gallet et al., 2020; Gallet et al., 2006; Gallet et al., 2008), Ebla in Northern Levant (Gallet et al., 2014; Gallet et al., 2008) and Tel Hazor in Southern Levant (Shaar et al., 2020; Shaar et al., 2016). However, although being key sites in Near Eastern archaeology, most of the data from these sites are not radiocarbon-dated. In this perspective, Tel Megiddo (Israel), with a radiocarbon-based age model covering the 3000-800 BCE time-span, is unique, providing unprecedented opportunity for stratigraphic, radiocarbon-calibrated archaeomagnetic time-series.

In the following we report the data of Tel Megiddo, which can be regarded as the largest archaeomagnetic intensity dataset from a single site. We compile the new data with nearby archaeomagnetic data derived mostly from radiocarbon-dated stratified mounds and historically-dated burnt structures to a single coherent continuous dataset that provides a sub-century resolution over millennial timescale. Based on the high-precision compilation, we calculate the Bayesian Levantine Archaeomagnetic intensity Curve (LAC). The LAC elucidates the details of the largest geomagnetic change in the Holocene, associated with the Levantine Iron Age Anomaly (Shaar et al., 2016) and the occurrence of geomagnetic spikes (Ben-Yosef et al., 2009; Shaar et al., 2011; Shaar et al., 2016). We use the LAC to enhance knowledge of the number, duration, and intensity of geomagnetic spikes, which define new robust upper limit constraints for both maximum field intensity and rate of change.

2 Materials and Methods

2.1 Tel Megiddo

Tel Megiddo (32.585N, 35.185E, Fig. 1) is a world-heritage archaeological site located on the western margins of the Jezreel Valley in northern Israel. Owing to its strategic location on the international route which connected Egypt with Mesopotamia, Megiddo was a central city and an important administration center through the Bronze and Iron Ages (ca. 3500 – 600 BCE). Extensive excavations of the mound have revealed more than thirty Bronze and Iron Age superimposed settlements, with several destruction layers marking violent endings in military campaigns (Finkelstein, 2009). The chronology of the entire Megiddo sequence was established from Bayesian analyses of ca. 150 radiocarbon samples (the total number of radiocarbon samples at Megiddo is 185) carefully collected from nearly all strata (Boaretto, 2022; Martin et al., 2020; Regev et al., 2014; Toffolo et al., 2014). Special care was taken in assembling the radiocarbon model from mostly short-lived organic material securely linked to the archaeological findings. The exceptionally large radiocarbon data from a detailed, continuous and well-established stratigraphy, along with the intensive ceramic record of Megiddo that defines the relative dating (e.g., late Iron I, early Iron IIA), provide a reliable absolute chronology of the Near Eastern archaeology.

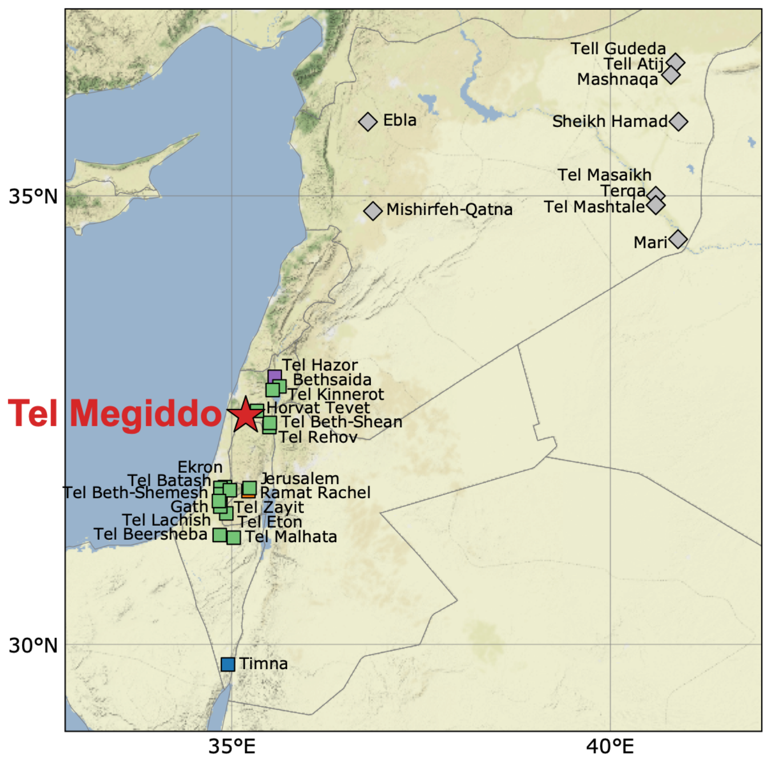

Figure 1: *Location map showing Tel Megiddo and other sites in the Levant and Western upper Mesopotamia used to construct the Levantine Archaeomagnetic Curve (LAC.v.1.0) shown in Fig. 6. Color code is as in Fig. 6.*

The archaeomagnetic stratigraphy of Tel Megiddo is based on twenty-three different contexts recovered from 18 layers excavated in six excavation areas (Fig. 2). Ten contexts (H-3/Q-2, Q-4, K-4/H-9/Q-7, H-11, K-6, H-15, S-2) are destruction layers with distinct boundaries and clear marks of their ending. From each context, we sampled fragments of indicative pottery with emphasis on local domestic material. We preferred, when possible, complete or cured vessels that were photographed and documented in the excavation reports. In three contexts (Q-4, Q-5, K-9) we also sampled fragments of cooking ovens (tabun). The samples discussed here include new data, as well as data already published in Shaar et al. (2016) and Shaar et al. (2020) who reported the initial archaeomagnetic stratigraphy of Megiddo. Supplementary Table S1 lists the archaeological details of all the material analyzed in this study.

a)

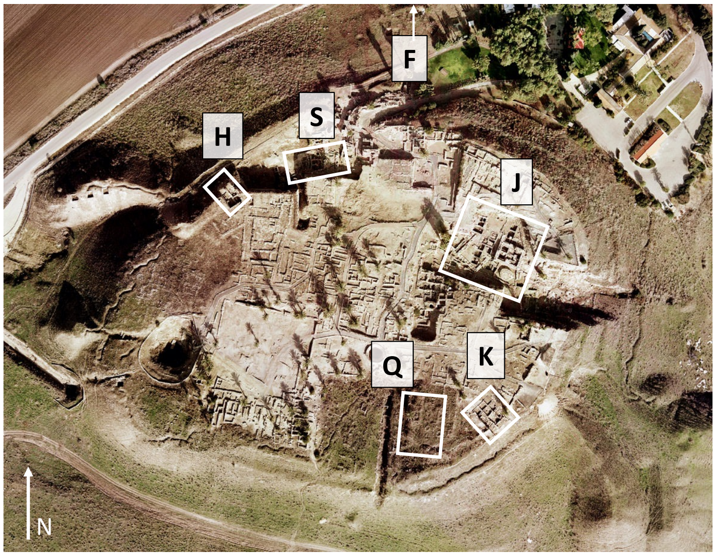

b)

Period \ Area	J	S	F	K	H	Q
Early Iron IIB					H-3	Q-2
Late Iron IIA						Q-4
Middle Iron IIA					H-7	Q-5
Early Iron IIA						Q-6
Late Iron I				K-4	H-9	Q-7
Middle Iron I					H-10	
Early Iron I					H-11	
Late Bronze III				K-6		
Late Bronze IIB				K-8		
Late Bronze IIA-IIB				K-9		
Late Bronze I			F-10		H-15	
Middle Bronze III				K-10		
Middle Bronze III				K-11		
Middle Bronze II			F-13			
Middle Bronze I		S-2				
Early Bronze III	J-6					
Early Bronze III	J-5					
Early Bronze IB	J-4					

Figure 2: Tel Megiddo. a) Air photo of the mound showing excavation areas discussed in the text. b) Tel Megiddo stratigraphy showing all strata analyzed for archaeointensity. Shaded cells mark destruction layers.

2.1 Experimental Design

Thellier-IZZI-MagIC paleointensity experiments were carried out in the shielded paleomagnetic laboratory at the Institute of Earth Sciences, The Hebrew University of Jerusalem, using two modified ASC TD-48 ovens and 2G-RAPID superconducting rock magnetometer (SRM). Specimens were prepared by gluing small pieces of pottery inside non-magnetic $22 \times 22 \times 20$ mm square alumina crucibles. The protocol followed the IZZI method (Tauxe & Staudigel, 2004; Yu et al., 2004) with routine pTRM checks at every second temperature step using an oven field of 40,50, or 60 μT. Heating time ranged from 40 to 65 minutes depending on the target temperature. In total, each IZZI experiment included 31 or 33 heating steps at 13 or 14 temperature intervals between 100°C to 590°C or 600°C. All specimens were subjected to anisotropy of thermoremanent magnetization (ATRM) experiments, which consisted of eight heating steps at 590°C or 600°C: a baseline zero-field step, six infield steps at orthogonal directions, and an additional alteration check. ATRM alteration parameter was calculated following Shaar et al. (2015) (Table 1). For specimens with ATRM alteration check > 6% anisotropy of anhysteretic remanent magnetization (AARM) was measured at 100mT AC field in 0.1mT DC bias field, at six orthogonal directions, after thermal demagnetization of the specimens. All specimens were subjected to cooling rate correction experiments, which consisted of 4-5 cooling steps from 590 °C or 600 °C to room temperature following the protocol described in Shaar et al. (2020). Archaeointensity values were calculated with the *Thellier-GUI* program (Shaar & Tauxe, 2013), incorporated into the *PmagPy* software package (Tauxe et al., 2016), using *Thellier Auto Interpreter* algorithm and the acceptance criteria listed in Table 1. Samples results are calculated by averaging at least 3 specimens per sample using the STDEV-OPT algorithm of the *Thellier-GUI* program and the 'extended error bounds" approach (Shaar & Tauxe, 2013; Shaar et al., 2016). When averaging samples data in 'groups' (section 3.1) we calculate a simple mean of the STDEV-OPT values of the samples. Detailed explanation on the methods can be found in Shaar et al. (2016) and Shaar et al. (2020). All measurements data are available in the MagIC databas (earthref.org/MagIC/19395). (note for reviewer/editor: The MagIC link will be activated only after publication and receiving DOI. Hence, we provide here a private link to the MagIC data, to be used during the review process. https://earthref.org/MagIC/19395/4406c155-3096-42e3-9e73-11ceac8580f2).

Table 1: Acceptance criteria, LAC.v.1.0

Criteria group *	Statistic	Threshold value	Description	Reference †
Specimen	FRAC	0.79	Fraction parameter	Shaar and Tauxe (2013)
	B	0.1	Scatter parameter	Coe et al. (1978); Selkin and Tauxe (2000)
	SCAT	True	Scatter parameter	Shaar and Tauxe (2013)
	GAP-MAX	0.5	maximum gap	Shaar and Tauxe (2013)
	N_{PTRM}	2	Number of pTRM checks	
	N	5	Number of data points	
	MAD	5	Maximum Angular Deviation of the zero field steps	Kirschvink (1980)
	DANG	10	Deviation Angle	Tauxe and Staudigel (2004)
	Alteration check (correction)	6%	Alteration check in TRM anisotropy and cooling rate experiments	Shaar et al. (2015)
Sample (pottery vessel, furnace, brick, slag)	N_{min}	3	Number of specimens	
	$N_{min\_aniso\_corr}$	at least half of the specimens	Minimum number of specimens with anisotropy correction	
	$N_{min\_cr\_corr}$	1	Minimum number of specimens with cooling rate correction	
	Σ	$\sigma <$ 3 μT OR σ % < 8%	Standard deviation of the sample mean	
	Anisotropy sample test	6%	If the mean anisotropy correction of all the specimens from the same sample (fragment) is higher than this value, specimens without anisotropy correction are discarded	

* For a complete description and definitions of paleointensity statistics see Paterson et al. (2014).

3 Results

3.1 Archaeomagnetic intensity stratigraphy of Tel Megiddo

The archaeomagnetic data from Tel Megiddo, including the data already published in Shaar et al. (2016) and Shaar et al. (2020) consists of 763 specimens from 175 samples (pottery fragments). In this study, we analyzed 288 specimens from 85 newly collected samples. In total, 583 specimens and 132 samples pass the criteria listed in Table 1, where archaeointensities obtained at the sample level are calculated from a minimum of 3 specimens. Fig. 3 shows representative cases of a successful specimen as well as interpretation failing criteria. The importance of the anisotropy and cooling rate corrections is illustrated in Fig. 4: typically, the bias due to anisotropy and cooling rate effects is 5%-15%; in some cases the combined correction exceeds 20%.

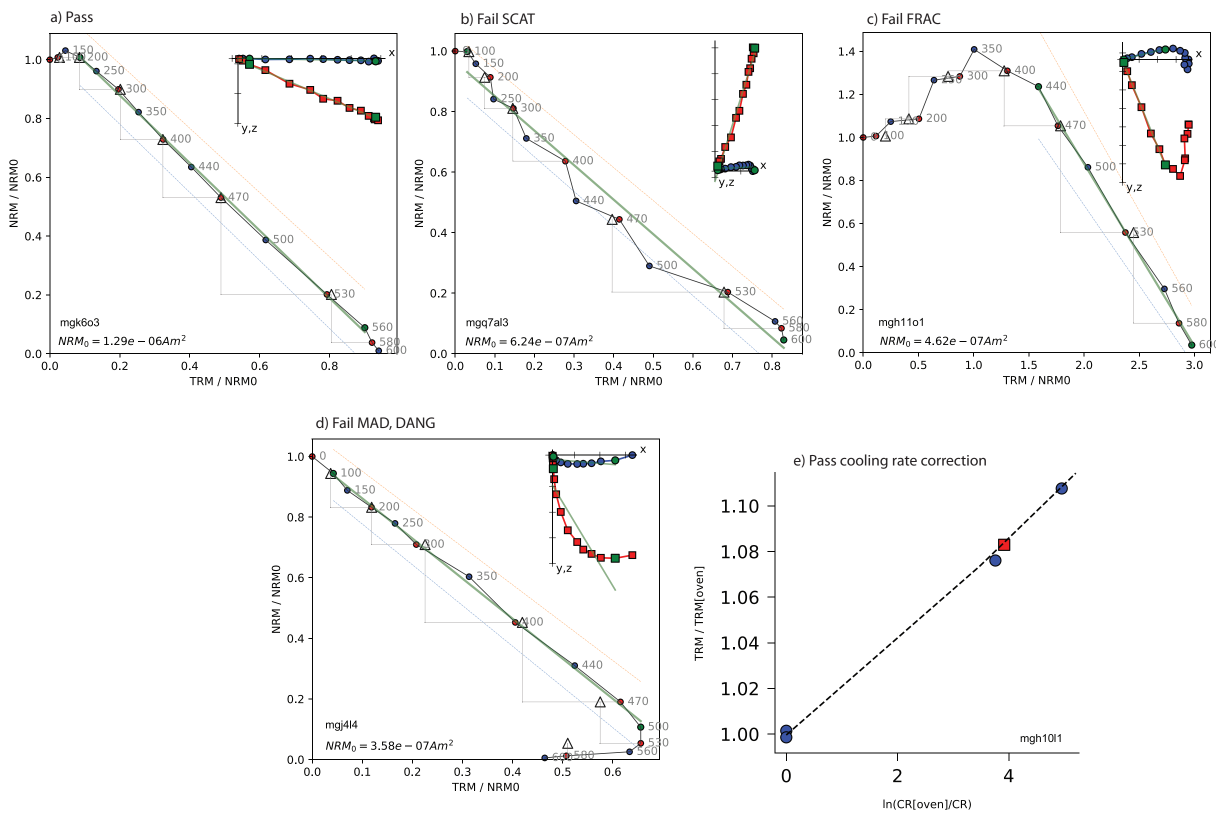

Figure 3: Representative results. (a-d) Red (blue) circles, and triangles in the main Arai plots are ZI steps, IZ steps, and pTRM checks, respectively. Blue (red) squares in the inset Zijderveld plots are x-y (x-z) projections of the NRMs remaining, where x axis is rotated to the direction of the NRM. Green line is the best-fit line. a) specimen passing all criteria. b-d) interpretations failing the SCAT (b), FRAC (c), MAD+DANG (d) criteria. e) successful cooling rate experiment. Blue circles are four measurements at three different cooling rates, red square is a projection of the ancient cooling rate on the best-fit line (dashed line).

Fig. 5 displays samples data with errors bars calculated using the "extended error bounds" approach (Shaar & Tauxe, 2013). In general, samples collected from the same archaeological context (termed hereafter 'group') show good agreement with only two outliers in group K-4 and Q-4. Levels H-9 and H-3 exhibit a large dispersion of data, with distinctively different values. As the ceramics in each context represent production during a time interval rather than a singular point in time, this probably indicates fast change in the field during the interval represented in the ceramic assemblage. Thus, we tentatively split the results from these two contexts to two sub groups in order to model the varying field. The mean archaeointensity of each group is calculated by averaging the sample means. Detailed samples data are given in Supplementary Table S2. Table 2 summarizes the groups data, including the archaeological affiliations and details on the radiocarbon data. We note that the age range we assign in Table 2 to each group (listed as 'model age range') is different than the radiocarbon age range in order to optimally represent the age range of the archaeological context considering the overall archaeological and historical constraints and the uncertainty associated with the production of the pottery in each archaeological layer. The archaeomagnetic stratigraphy shown in Fig. 5 (Table 2) shows an exceptionally large amplitude changes - between 39 to 90 μT - with few significant oscillations. In the following sections we explore in details the extreme amplitude change depicted by Megiddo data.

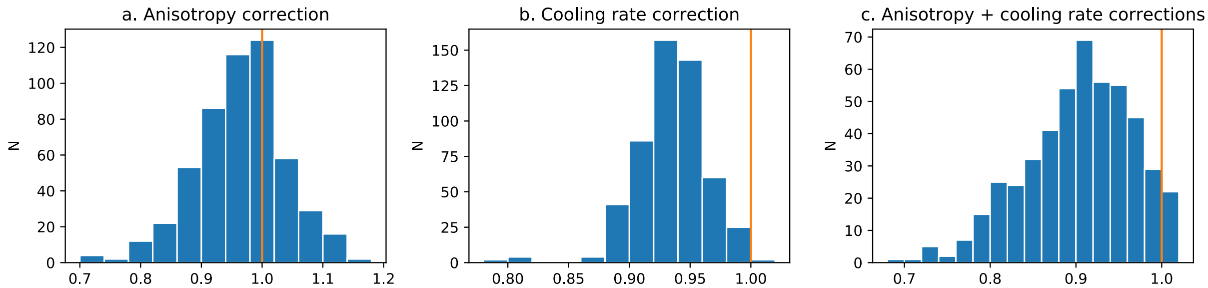

Figure 4: Histograms of anisotropy and cooling rate corrections.

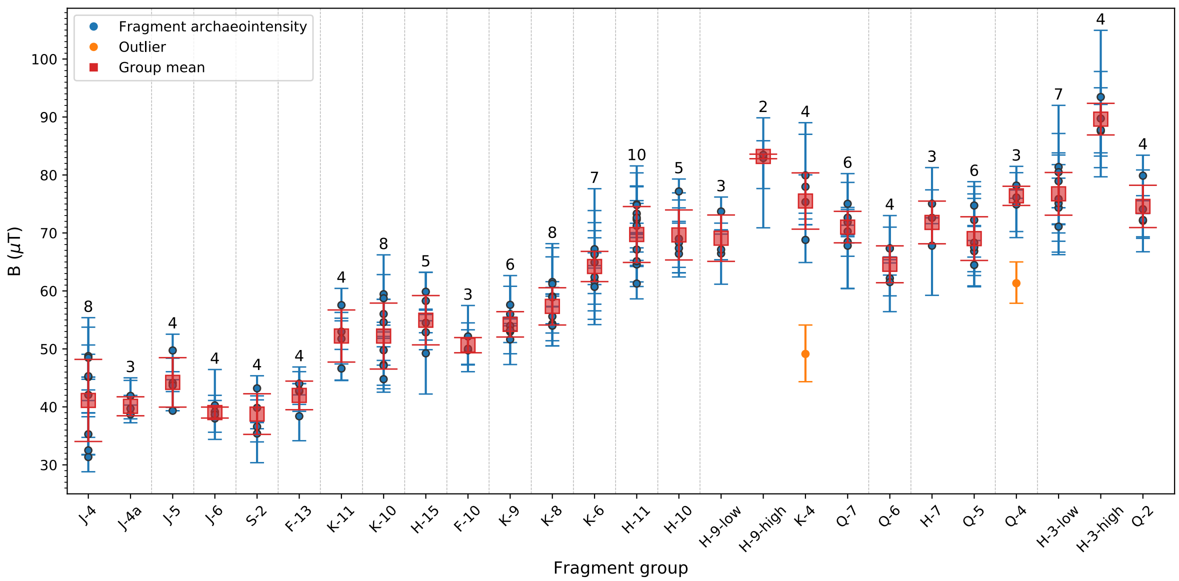

Figure 5: Archaeomagnetic stratigraphy of Tel Megiddo constructed from 132 samples. Filled circles (red squares) show archaeointensity of samples (groups means). Number of samples used to calculate group mean is shown above each error-bar. Vertical lines represent chrono-stratigraphic division. Fragments (samples) groups are plotted according to the relative age.

Table 2: Archaeointensity results, Tel Megiddo

Megiddo Group	**name in LAC.v.0.1***	**Radiocarbon age BCE 68.2% probability interval (95.4 % probability interval) †**	**Model Age Range (BCE) ‡**	**N samples**	**n specimens**	**B (μT)**	**B σ (μT)**	**VADM (ZAm^2)**	**VADM σ (ZAm^2)**
Q-2	mgq02	801-756 (805-735); Assyrian destruction level	820-732	4	15	74.6	3.6	140.3	6.9

H-3-low	mgh03-low	-	820-732	7	37	76.7	3.7	144.3	6.9
H-3-high	mgh03-high			4	18	89.6	2.7	168.6	5.1
Q-4	mgq04	897-821 (901-809)	880-840	3	14	76.4	1.7	143.7	3.1
Q-5	mgq05	956-894 (967-848)	925-875	6	30	69	3.8	129.8	7.1
H-7	Mgh07	930-900 (945-860)	925-875	3	16	71.8	3.7	135.1	6.9
Q-6	mgq06	979-911 (989-876)	950-900	4	16	64.6	3.2	121.5	6
Q-7	mgq07	1047-975 (1052-946)	1050-950	6	18	71	2.7	133.5	5.1
H-9-low	mgh09-low	1038-976 (1056-936)	1050-950	3	15	69.1	4	129.9	7.5
H-9-high	mgh09-high			2	9	83.2	0.4	156.5	0.7
K-4	mgk04	1037-951 (1053-908)	1050-950	4	15	75.5	4.9	142	9.1
H-10	mgh10	1068-1031 (1087-1023)	1100-1025	5	15	69.7	4.3	131	8.1
H-11	mgh11	1105-1051 (1115-1041)	1125-1075	10	30	69.7	4.8	131.1	9.1
K-6	mgk06	1148-1123 (1168-1104)	1175-1125	7	31	64.2	2.6	120.8	4.9
K-8	mgk08	1238-1178 (1268-1158)	1250-1175	8	33	57.3	3.2	107.8	6
K-9	mgk09	1323-1230 (1381-1201)	1400-1250	6	20	54.2	2.2	102	4.1
F-10	mgf10	1545-1354 (1561-1313)	1550-1400	3	14	50.6	1.3	95.2	2.5
H-15	mgh15	1557-1509 (1572-1463)	1550-1475	5	25	54.9	4.3	103.3	8
K-10	mgk10	1581-1545 (1596-1535)	1600-1550	8	35	52.2	5.7	98.2	10.7
K-11	mgk11	1626-1579 (1643-1561)	1650-1600	4	21	52.2	4.5	98.2	8.4
F-13	mgf13	-	1900-1700	4	25	42	2.5	78.9	4.6
S-2	mgs02	1942-1902 (1965-1886)	1950-1900	4	12	38.8	3.5	72.9	6.6
J-6	mgj06	2860-2540 (2880-2450)	2850-2500	4	15	39	0.9	73.4	1.8
J-5	mgj05	2920-2720 (2970-2670)	2900-2800	4	12	44.2	4.3	83.2	8
J-4 §	mgj04	3060-2880 (3180-2830)	3100-2900	8	46	41.1	7.1	77.3	13.3
J-4a §	mgj04a	3060-2880 (3180-2830)	3100-2900	3	10	40.1	1.6	75.4	3.1

* Name in model data (Supplementary Table S9)

† Radiocarbon date from Regev et al. (2014) ; Toffolo et al. (2014)**;** Martin et al. (2020); Boaretto (2022); There are no radiocarbon data from H-03 and the age is linked to the Assyrian destruction level. Ages from S-2 are preliminary. There are no radiocarbon data from F-13 and age is inferred from correlation to strata in areas K,S.

‡ Age range used in LAC.v.1.0

§ J-4 and J-4a are two groups from the same level. J-4a fragments were collected from loci representing the end-days of the temple, whereas the J-4 items originated from a fill context.

3.2 Levantine archaeomagnetic curve (LAC.v.1.0)

In an effort to minimize uncertainties associated with differences in laboratory techniques, data analysis approaches, and selection criteria (see review in Shaar et al. (2020)), our compilation of the Levant and Upper Mesopotamia is based on data obtained using the Thellier-IZZI-MagIC method (Shaar & Tauxe, 2013; Tauxe & Staudigel, 2004) with the criteria defined in Shaar et al. (2016, 2020), and the Triaxe method (Le Goff & Gallet, 2004). These two methods were tested against each other in a blind test and proved to be equivalent (Shaar et al., 2020). Also included data obtained by Genevey et al. (2003) that applied the Thellier-Coe method (Coe et al., 1978) because these data were tested against the Triaxe in Gallet and Le Goff (2006). We include in the compilation only groups that include at least two samples with overlapping intensity error bars, after inspection for outliers, where a group is defined as archaeological context, locus, level, stratum, burnt building, and slag layer. Fig. 6 displays data from 142 groups between 3000 – 500 BCE passing these criteria. Data are displayed in terms of virtual axial dipole moment (VADM) – a transformation from local, latitude-dependent field intensity measurement to the equivalent geomagnetic axial dipole moment (Tauxe et al., 2018). The data from Syria, representing Mesopotamia and Northern Levant (Gallet & Al-Maqdissi, 2010; Gallet & Butterlin, 2015; Gallet et al., 2014; Gallet et al., 2020; Gallet et al., 2006; Gallet et al., 2008; Genevey et al., 2003; Livermore et al., 2021), are displayed as published with few updates on the ages of some fragment groups (see Supplementary Material) . Data from Timna-30 slag mound (Shaar et al., 2011), Tel Hazor (Shaar et al., 2016), and the Judean stamped jars (Ben-Yosef et al., 2017), which were published as samples, are shown here as group means (Supplementary Tables S3-S8). We note few updates on the ages of some of these published data (see Supplementary Material for details): We arrange the data from strata V-VI in Tel Hazor (Shaar et al., 2016) in three distinct groups based on sub-division to phases and re-assign their ages accordingly (Supplementary Table S3). The Bayesian age model of Timna-30 slag mound (Shaar et al., 2011), which was originally established using magnetostratigraphic correlation with Khirbet En Nahas (Ben-Yosef et al., 2009) is revised here, and now includes only radiocarbon samples collected from Timna-30

(Supplementary Tables S5-S7). Also, the age range of the Judean stamped handles is extended from Ben-Yosef et al. (2017) following Vaknin et al. (submitted) (Supplementary Table S8).

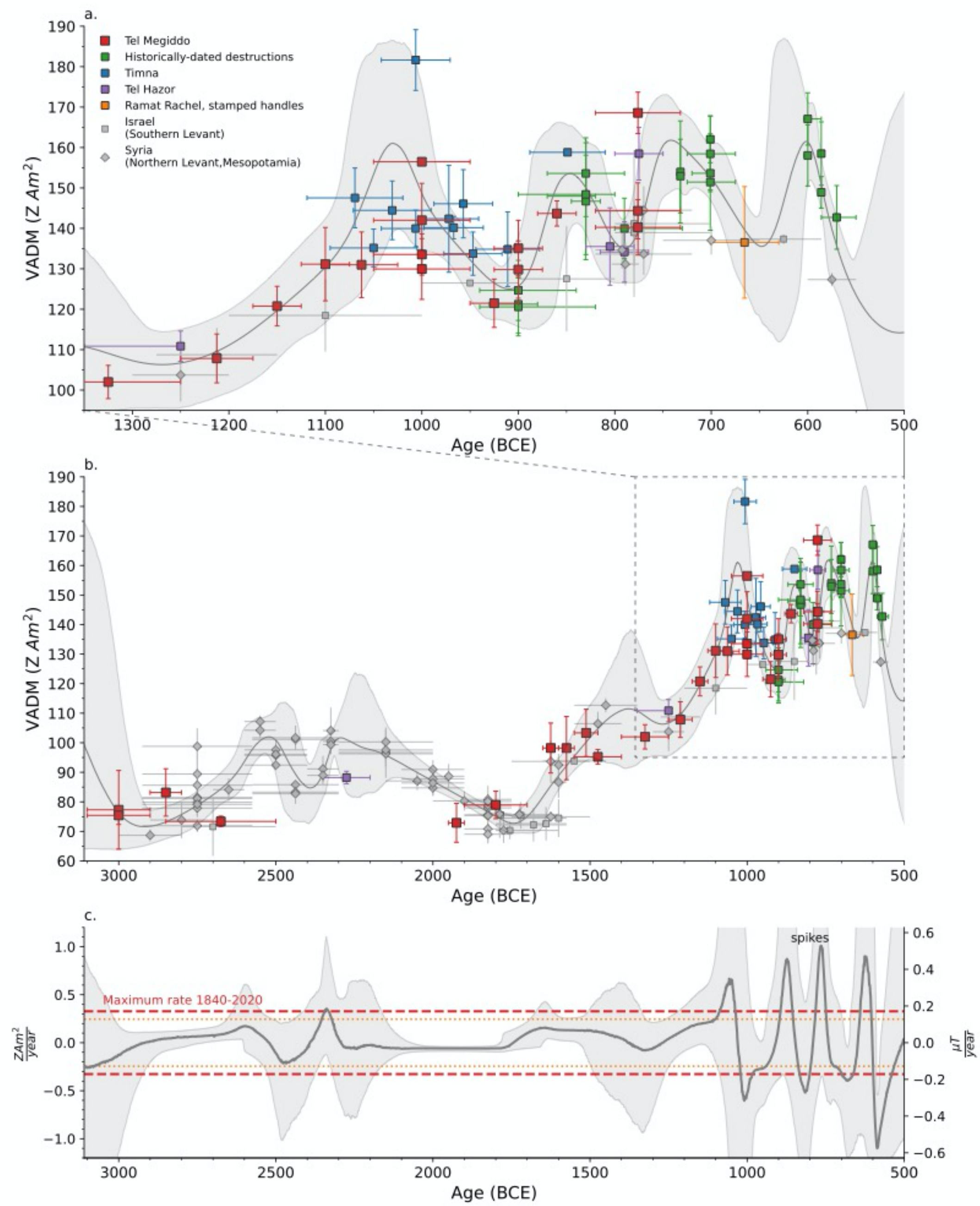

Figure 6: Archaeointensity curve. a,b) Levantine archaeomagnetic intensity curve (LAC.v.1.0). Colored symbols are groups of samples directly dated with radiocarbon and/or by clear association to dated historical events. Gray symbols represent groups dated using various archaeological methods. From the 17^{th} to the 6^{th} centuries there is at least one directly-dated context per century. Curve and shaded area in (a-b) are the average and the 95% credible interval calculated using the AH-RJMCMC algorithm (Livermore et al., 2018). c) Rate of change. Dashed red and dotted orange lines show the maximum rate between 1840-2020 and the maximum rate in today's field (Fig. 7), respectively. The oscillation pattern shown in (a) includes four spikes with VADM >150 ZAm^2 and rate of change of 0.35-0.55 μT/year (c).

The data from Tel Megiddo, obtained from materials that are directly linked to the radiocarbon-dated contexts (red symbols in Fig. 6) form the skeleton of the archaeomagnetic dataset with a time series of well-established chronological anchors. These data are combined with other radiocarbon archaeomagnetic contexts from Tel Hazor and Timna (shown in colored symbols is Fig. 6) as well as with a newly published dataset obtained from burnt structures destroyed during historically-dated military campaigns (Vaknin et al., 2020; Vaknin et al., submitted). The burnt structures are crucial tie points for two reasons. First, the uncertainty in radiocarbon ages during the late Iron Age is in the order of 200-400 years due to the plateau in the calibration curve (Reimer et al., 2020), while the dates of the historical campaigns are unique in their precision. Second, the burnt structures record a single event, as the fire during the destruction resets the magnetization in the bricks, compared to the ceramic groups that provide data over a time interval representing a production period. Taken together, the period between 1700-550 BCE in the Levant and western upper Mesopotamia is now represented by 87 archaeomagnetic contexts, 57 of which are dated using radiocarbon and/or direct association with historically-dated secure events. All the directly-dated contexts (highlighted in colors in Fig. 6) are spread in such a way that there is at least one context per century after 1700 BCE, providing a robust century-scale (or better) resolution.

With the data described above, and summarized in Supplementary Table S9, we calculate a Bayesian curve with its corresponding 95% credible envelope (Fig. 6, Supplementary Table S10). We term this curve 'Levantine Archaeomagnetic Curve version 1.0', or LAC.v.1.0. The LAC is calculated using the age hyperparameter reverse-jump Monte Carlo Markov Chain (AH-RJMCMC) algorithm developed by Livermore et al. (Livermore et al., 2018)(https://github.com/plivermore/AH-RJMCMC1). The algorithm is based on piece-wise linear extrapolation between vertices drawn in a random-walk like perturbation within a space allowed by acceptance criteria. The prior assumptions of the model are as follows: i) the allowed range of vertices VADM values is between 60 to 200 ZAm^2; ii) the allowed number of vertices (K) is between $K_{min} = 1$ to $K_{max} = 150$; iii) ages in all contexts are uniformly distributed except the ages of Timna, which were modeled as normal distribution; iv) groups mean and standard deviation define a normal distribution of archaeointensity data. In addition, Supplementary Table S9 defines a stratigraphic order for contexts collected from the layered sites (Tel Megiddo, Tel Hazor, Tell Atij, Tell Tel Gudeda, and Timna slag mound) as well as for some of the destructions levels in Vaknin et al. (submitted). The model uses the following parameters: $\sigma_{move} = 30$ yrs, $\sigma_{change} = 10$ Z Am^2, and $\sigma_{birth}=10$ Z Am^2, which define the distributions of a vertex move in age, vertex change in intensity, and intensity of a new vertex born with respect to the extrapolated intensity at the vertex age; each perturbation includes one age resampling of data in each perturbation (num_age_changes = 1); chain length is $2 \cdot 10^8$.

4 Discussion

4.1 What is the highest geomagnetic field intensity?

Considering all the published paleointensity estimates from individual samples (i.e. not group means) from the past 5 My available in the GEOMAGIA50 (Brown et al., 2015) and PINT (Biggin et al., 2009; Bono et al., 2022) databases, only 1% of the data show VADM > 150 ZAm^2 and they are sporadically scattered. As such, VADM values calculated from global geomagnetic models do not exceed 140 ZAm^2 (Arneitz et al., 2019; Constable et al., 2016; Korte & Constable, 2018; Panovska et al., 2019; Pavon-Carrasco et al., 2014). The only exception is the time interval between the end of the 2nd millennium BCE and the middle of the 1st millennium BCE, where a significant number of observations point to unusually high field values at several locations in Eurasia (Ben-Yosef et al., 2017; Cai et al., 2017; Di Chiara et al., 2014; Ertepinar et al., 2012; Kissel et al., 2015; Molina-Cardin et al., 2018; Shaar et al., 2011; Shaar et al., 2017; Shaar et al., 2016; Vaknin et al., 2020). This high field episode is probably associated with a more complex field structure than today's (Korte & Constable, 2018; Osete et al., 2020) and presumably with a local high field anomaly in the Near East termed 'Levantine Iron Age Anomaly' (LIAA) (Shaar et al., 2018; Shaar et al., 2017; Shaar et al., 2016). The highest VADM values, representing the climax of the LIAA were termed 'geomagnetic spikes' by Ben-Yosef et al. (2009) and Shaar et al. (2011). Livermore et al. (2021) raised the question of the robustness of the spikes and pointed out that the number of spikes and their values are strongly dependent on the archaeomagnetic data used, in particular the experimental errors and the averaging scheme adopted (i.e. samples groups versus individual samples). Here, we address the issues raised by Livermore et al. (2021) and assemble a much denser dataset, which is based solely on group averages. This way, each data point in our compilation represents exactly the same quantity and gain the same weight in the Bayesian calculation process. The new curve shows the occurrence of four spikes with peak VADM of 155-162 Z Am^2 around 1000, 850, 750, and 600 BCE. Each spike is represented by several coeval or nearly coeval groups, where overall, fourteen groups have VADM > 150 Z Am^2. It should be noted that the same series of four spikes is obtained if only radiocarbon-dated data are used for the construction of the curve, as well as those related to historically-dated destruction layers. Considering that each group represents a time-average of several samples, we suggest a value of 155 Z Am^2 as a robust and conservative upper limit for maximum field value. Yet, based on samples data, it is still possible that highest values may have occurred for a short time interval.

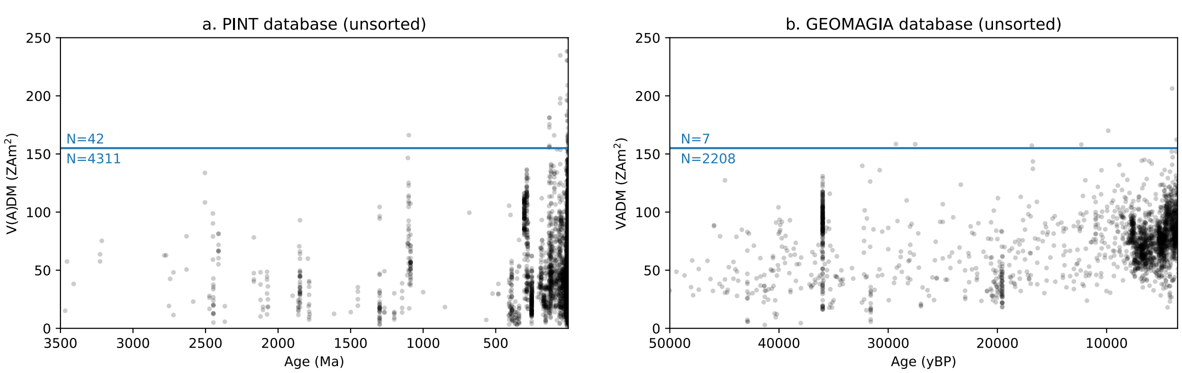

Figure 7: Comparison of spikes paleointensity with the global databases. a) PINT database (Bono et al., 2022). b) GEOMAGIA50 (Brown et al., 2015) before 3500 yBP. Data were not screened out by any criteria and shown as are. Horizontal lines show the value of 155 ZAm^2 corresponding to the lowest spikes according to LAC.v.1.0 (Fig. 6). N is the number of paleointensity estimates below and above 155 ZAm^2.

Figure 7 demonstrates that spike-like values are rare in the paleomagnetic record, showing all the published absolute paleointensity data with age older than 1500 BCE from the GEOMAGIA50 and PINT databases. Only 49 data points out of 6568 have field values higher than 155 Z Am^2, none of which pass the rather strict statistical tests applied in the LAC. Given the specific conditions associated with the Levantine geomagnetic spikes, the difficulty in detecting similar high paleointensity values in the global paleointensity record is not surprising. First, our dense dataset that includes on average 10 archaeointensity groups (each consists of at least 3 samples) per century during the high-field interval (Fig. 6a) shows that the duration of the spikes is not more than a century. Thus, if an average of several samples is required to obtain a robust paleointensity estimate, a large dataset, such as the LAC dataset, is required to detect spikes. Second, global geomagnetic models indicate that the geomagnetic dipole during the spikes episode is most likely the highest in the Holocene (Constable et al., 2016; Pavon-Carrasco et al., 2014; Schanner et al., 2022). Thus, the likelihood of detecting spikes may depend on the likelihood that the ancient paleomagnetic dipole was as similarly high. Third, the spikes is a regional feature associated with a local geomagnetic anomaly, which is expressed not only by high field values, but also by directional deviations from a dipole field (Osete et al., 2020; Shaar et al., 2018; Shaar et al., 2016). Taken altogether, there are low chances that the scattered and sparse paleointensity database spanning the geological record can reveal short-lived spikes. Moreover, from the comparison with the global paleointensity database we can conclude that spikes represent the highest value the geomagnetic field can reach and can serve as a robust upper boundary for the maximum strength of the geomagnetic field at a given location,

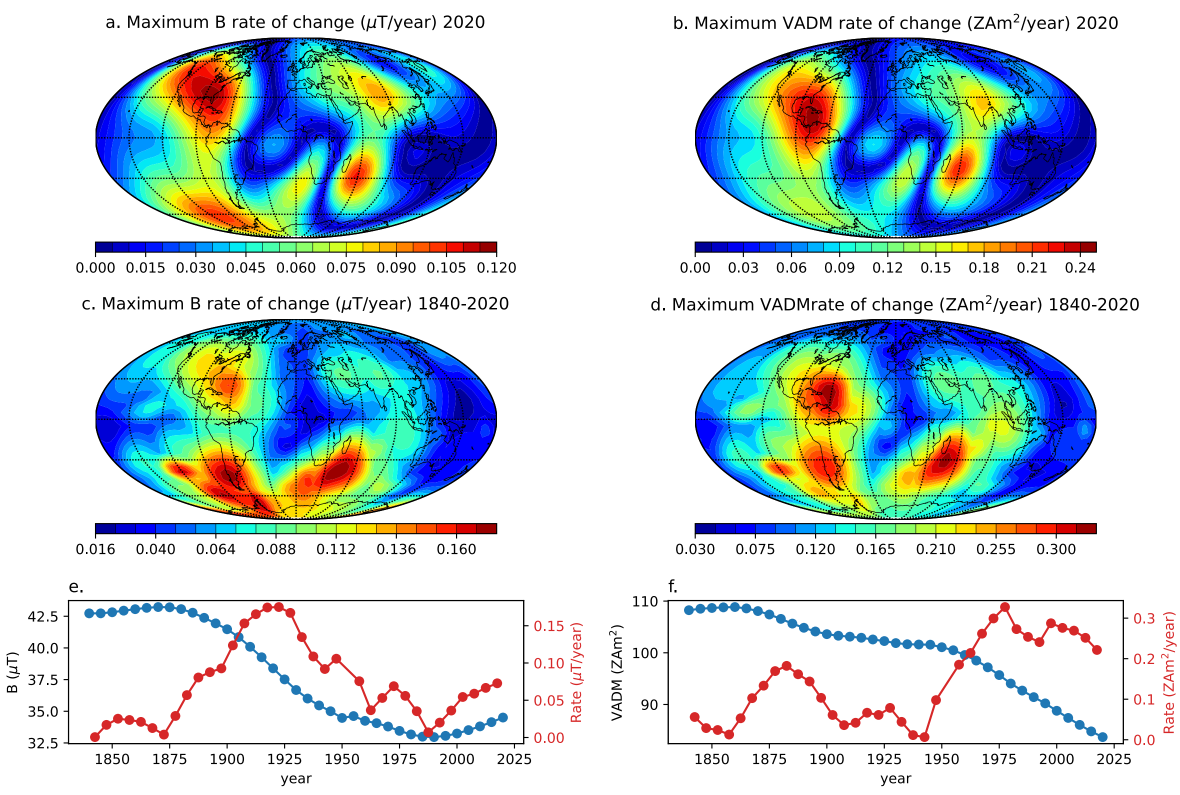

Figure 8: Maximum rate of change of the geomagnetic field intensity between 1840-2020. a-b) Intensity and VADM rate of change in toady's field calculated from IGRF13 model (Alken et al., 2021) epochs 2020,2015. c-d) Maximum intensity and VADM rate of change between 1840-2020 calculated from IGRF models (Alken et al., 2021) between 1950-2020 and gufm1 model (Jackson et al., 2000) between 1840-1950. e) Field intensity and rate of change at the location with the maximum B change (40°S, 45°E). f) VADM and rate of change at the location with the maximum VADM change (20°N, 65°W).

4.2 What is the maximum rate of geomagnetic field changes?

We inspect now the rate of change of the geomagnetic field. The rates associated with the spikes range between ~0.35 – 0.55 μT/year, or 0.7 – 1.1 Z Am^2/year in VADM values. To place these values within the context of the global geomagnetic field behavior, we calculate in Fig. 8 the maximum rate in today's field by looking at the difference between IGRF models epochs 2015 and 2020 (Alken et al., 2021). On most of Earth surface the rates do not exceed 0.1 μT/year (~0.2 Z Am^2/year) and a maximum rate of 0.12 μT/year occurs only in limited areas. VADM transformation that accounts for the latitudinal dependency of the field yields a maximum rate of 0.25 Z Am^2/year. We expand the calculation back to 1840 using the gufm1 model (Jackson et al., 2000) for years 1840-1950 and IGRF models for years 1950-2020 (Alken et al., 2021), by looking at the maximum difference in field intensity every 5 years at any point on Earth surface. The maximum rate of change during the past 190 years is not significantly different than today: 0.18 μT/year or 0.33 Z Am^2/year. These rates are thus significantly lower than the rates observed during the spikes time interval. Hence, LAC.v.1.0 also places new robust constraints for how fast the field can change.

We note that the rates calculated using LAC.v.1.0 appear more moderate than first considered in previous studies (Ben-Yosef et al., 2009; Shaar et al., 2011), which had raised questions regarding the dynamo processes behind them (Livermore et al., 2014; Troyano et al., 2020). Although the spikes are now within the range of variations permitted by our current understanding of the geodynamo (Davies & Constable, 2017; Davies & Constable, 2018; Livermore et al., 2014), the fluctuations associated with spikes remain unprecedented in their amplitude and rate.

4.3 Long term evolution of the Levantine Iron Age Anomaly

The archeo-magnetostratigraphy of Tel Megiddo reveals the Holocene greatest amplitude change at multi-century scales between 1750 BCE to 1000 BCE. The increase began with a minimum of 73 Z Am^2 in the 18th century BCE - a period characterized by the lowest intensities in the Near East over the last five millennia, comparable to the low values at the beginning of the 3rd millennium BCE (Fig. 6b). The 700 years-long increase is nearly continuous, punctuated by a century-scale peak around 1500 BCE. The spike period may be, therefore, a climax of a long-term evolution in geomagnetic field intensity in the Near East, which could result from the occurrence of intense and rapidly evolving flux bundles at the core-mantle boundary. It also contrasts with the period spanning from the third millennium BCE to the 18th century BCE, which shows intensity peaks of moderate amplitude associated with lower rates of change of less than 0.2 μT/year (Figs. 6b,c; see also Gallet et al. (2020)). The significant increase in intensity would then result in spikes instead of intensity peaks, with the first events also being shorter and apparently more frequent, which could reflect a remarkable change in core dynamics.

5 Conclusions

We report here archaeomagnetic data from Tel Megiddo, which can be considered as the largest archaeomagnetic dataset from a single site, with 23 groups of indicative pottery collected from 18 consecutive radiocarbon-dated archaeological strata.

We assemble a new archaeomagnetic compilation of the Levant and Western Upper Mesopotamia between 3000 BCE to 550 BCE with 142 different groups of samples. The interval 1700 BCE to 550 BCE is based mostly on contexts that are directly dated using radiocarbon and/or clear association with historical dating, providing an unprecedented sub-century resolution over long millennial timescale. We use this compilation to calculate the Levantine Archaeomagnetic Curve (LAC.v.1.0) – a Bayesian regional curve for high-precision archaeomagnetic dating.

The LAC depicts four geomagnetic spikes between 1050 BCE to 600 BCE, defining new upper limits for both the maximum local field values and rate of change. Considering the overall uncertainty, we suggest 155 ZAm^2 and 0.5 μT/year (1 ZAm2/year in VADM values) as conservative upper boundaries for these quantities.

As a concluding remark we highlight the challenge in constructing a robust continuous geomagnetic intensity curve at a sub-centennial resolution over a large time interval. This is made possible in this study by exploiting the advantage of the Near East that allows acquisition of large multiple archaeomagnetic datasets, with precise dating, stratigraphic constraints, and cross-correlation between sites. In this respect, Tel Megiddo is an exemplary case study demonstrating a strong link between archaeology, radiocarbon and geomagnetism.

Acknowledgments

Project has received funding from the European Research Council (ERC) under the European Union’s Horizon 2020 research and innovation programme (grant agreement No 804490) to RS. The study was partly supported by the Israel Science Foundation (ISF) grant 1364/15 to RS. This study was partly financed by INSU-CNRS program PNP to YG. Work on the Megiddo samples was supported by the Dan David Foundation and grants from Mark Weissman and Jacques Chahine to IF. We thank Phil Livermore for assisting with the AH-RJMCMC analysis.

Open Research

All measurements data are available in the MagIC database (earthref.org/MagIC/19395)

References

Alken, P., Thebault, E., Beggan, C. D., Amit, H., Aubert, J., Baerenzung, J., et al. (2021). International Geomagnetic Reference Field: the thirteenth generation. *Earth Planets and Space, 73*(1) https://doi.org/10.1186/s40623-020-01288-x

Arneitz, P., Egli, R., Leonhardt, R., & Fabian, K. (2019). A Bayesian iterative geomagnetic model with universal data input: Self-consistent spherical harmonic evolution for the geomagnetic field over the last 4000 years. *Physics of the Earth and Planetary Interiors, 290*, 57-75 https://doi.org/10.1016/j.pepi.2019.03.008

Arneitz, P., Leonhardt, R., Schnepp, E., Heilig, B., Mayrhofer, F., Kovacs, P., et al. (2017). The HISTMAG database: combining historical, archaeomagnetic and volcanic data. *Geophysical Journal International, 210*(3), 1347-1359 https://doi.org/10.1093/gji/ggx245

Ben-Yosef, E., Millman, M., Shaar, R., Tauxe, L., & Lipschits, O. (2017). Six centuries of geomagnetic intensity variations recorded by royal Judean stamped jar handles. *Proceedings of the National Academy of Sciences of the United States of America, 114*(9), 2160-2165 https://doi.org/10.1073/pnas.1615797114

Ben-Yosef, E., Tauxe, L., Levy, T. E., Shaar, R., Ron, H., & Najjar, M. (2009). Geomagnetic intensity spike recorded in high resolution slag deposit in Southern Jordan. *Earth and Planetary Science Letters, 287*(3-4), 529-539 https://doi.org/10.1016/j.epsl.2009.09.001

Biggin, A. J., Strik, G. H. M. A., & Langereis, C. G. (2009). The intensity of the geomagnetic field in the late-Archaean: new measurements and an analysis of the updated IAGA palaeointensity database. *Earth Planets and Space, 61*(1), 9-22 https://doi.org/10.1186/Bf03352881

Boaretto, E. (2022). Radiocarbon dating. In M. A. S. Martin & I. Finkelstein (Eds.), *Megiddo VI: The 2010-2014 Seasons*. PA: State College.

Bono, R. K., Paterson, G. A., van der Boon, A., Engbers, Y. A., Grappone, J. M., Handford, B., et al. (2022). The PINT database: a definitive compilation of absolute palaeomagnetic intensity determinations since 4 billion years ago. *Geophysical Journal International, 229*(1), 522-545 https://doi.org/10.1093/gji/ggab490

Brown, M. C., Donadini, F., Korte, M., Nilsson, A., Korhonen, K., Lodge, A., et al. (2015). GEOMAGIA50.v3: 1. general structure and modifications to the archeological and volcanic database. *Earth Planets and Space, 67*, 1-31 https://doi.org/10.1186/s40623-015-0232-0

Brown, M. C., Herve, G., Korte, M., & Genevey, A. (2021). Global archaeomagnetic data: The state of the art and future challenges. *Physics of the Earth and Planetary Interiors, 318* https://doi.org/10.1016/j.pepi.2021.106766

Cai, S. H., Jin, G. Y., Tauxe, L. S., Deng, C. L., Qin, H. F., Pan, Y. X., & Zhu, R. X. (2017). Archaeointensity results spanning the past 6 kiloyears from eastern China and implications for extreme behaviors of the geomagnetic field. *Proceedings of the National Academy of Sciences of the United States of America, 114*(1), 39-44 https://doi.org/10.1073/pnas.1616976114

Campuzano, S. A., Gomez-Paccard, M., Pavon-Carrasco, F. J., & Osete, M. L. (2019). Emergence and evolution of the South Atlantic Anomaly revealed by the new paleomagnetic reconstruction SHAWQ2k. *Earth and Planetary Science Letters, 512*, 17-26 https://doi.org/10.1016/j.epsl.2019.01.050

Coe, R., Gromme, S., & Mankinen, E. (1978). Geomagnetic paleointensities from radiocarbon-dated lava flows on Hawaii and question of Pacific nondipole low. *Journal of Geophysical Research*, 1740-1756 https://doi.org/10.1029/JB083iB04p01740

Constable, C., Korte, M., & Panovska, S. (2016). Persistent high paleosecular variation activity in southern hemisphere for at least 10 000 years. *Earth and Planetary Science Letters, 453*, 78-86 https://doi.org/10.1016/j.epsl.2016.08.015

Courtillot, V., & Le Mouel, J. L. (2007). The study of earth's magnetism (1269-1950): A foundation by peregrinus and subsequent development of geomagnetism and paleomagnetism. *Reviews of Geophysics, 45*(3) https://doi.org/10.1029/2006rg000198

Davies, C., & Constable, C. (2017). Geomagnetic spikes on the core-mantle boundary. *Nature Communications, 8* https://doi.org/10.1038/ncomms15593

Davies, C. J., & Constable, C. G. (2018). Searching for geomagnetic spikes in numerical dynamo simulations. *Earth and Planetary Science Letters, 504*, 72-83 https://doi.org/10.1016/j.epsl.2018.09.037

Di Chiara, A., Tauxe, L., & Speranza, F. (2014). Paleointensity determination from Sao Miguel (Azores Archipelago) over the last 3 ka. *Physics of the Earth and Planetary Interiors, 234*, 1-13 https://doi.org/10.1016/j.pepi.2014.06.008

Ertepinar, P., Langereis, C. G., Biggin, A. J., Frangipane, M., Matney, T., Okse, T., & Engin, A. (2012). Archaeomagnetic study of five mounds from Upper Mesopotamia between 2500 and 700 BCE: Further evidence for an extremely strong geomagnetic field ca. 3000 years ago. *Earth and Planetary Science Letters, 357*, 84-98 https://doi.org/10.1016/j.epsl.2012.08.039

Finkelstein, I. (2009). Destructions: Megiddo as a case study. In J. D. Schloen (Ed.), *Exploring the Longue Durée* (pp. 113-126). Indiana: Eisenbrauns.

Gallet, Y., & Al-Maqdissi, M. (2010). Archeomagnetism in Mishirfeh-Qatna: New data on the evolution of intensity in the earthly magnetic field in the Middle East during the last millenia. *Akkadica, 131*(1), 29-46

Gallet, Y., & Butterlin, P. (2015). Archaeological and geomagnetic implications of new archaeomagnetic intensity data from the Early Bronze High Terrace "Massif Rouge' at Mari (Tell Hariri, Syria). *Archaeometry, 57*, 263-276 https://doi.org/10.1111/arcm.12112

Gallet, Y., D'Andrea, M., Genevey, A., Pinnock, F., Le Goff, M., & Matthiae, P. (2014). Archaeomagnetism at Ebla (Tell Mardikh, Syria). New data on geomagnetic field intensity variations in the Near East during the Bronze Age. *Journal of Archaeological Science, 42*, 295-304 https://doi.org/10.1016/j.epsl.2017.11.013

Gallet, Y., Fortin, M., Fournier, A., Le Goff, M., & Livermore, P. (2020). Analysis of geomagnetic field intensity variations in Mesopotamia during the third millennium BC with archeological implications. *Earth and Planetary Science Letters, 537* https://doi.org/10.1016/j.epsl.2020.116183

Gallet, Y., Genevey, A., Le Goff, M., Fluteau, F., & Ali Eshraghi, S. (2006). Possible impact of the Earth's magnetic field on the history of ancient civilizations. *Earth and Planetary Science Letters, 246*(1-2), 17-26 https://doi.org/10.1016/j.epsl.2006.04.001

Gallet, Y., & Le Goff, M. (2006). High-temperature archeointensity measurements from Mesopotamia. *Earth and Planetary Science Letters, 241*(1-2), 159-173 https://doi.org/10.1016/j.epsl.2005.09.058

Gallet, Y., Le Goff, M., Genevey, A., Margueron, J., & Matthiae, P. (2008). Geomagnetic field intensity behavior in the Middle East between similar to 3000 BC and similar to 1500 BC. *Geophysical Research Letters, 35*(2) https://doi.org/10.1029/2007gl031991

Genevey, A. S., Gallet, Y., & Margueron, J. C. (2003). Eight thousand years of geomagnetic field intensity variations in the eastern Mediterranean. *Journal of Geophysical Research-Solid Earth, 108*(B5) https://doi.org/10.1029/2001jb001612

Jackson, A., Jonkers, A. R. T., & Walker, M. R. (2000). Four centuries of geomagnetic secular variation from historical records. *Philosophical Transactions of the Royal Society of London Series a-Mathematical Physical and Engineering Sciences, 358*(1768), 957-990 https://doi.org/10.1098/rsta.2000.0569

Kirschvink, J. L. (1980). The Least-Squares Line and Plane and the Analysis of Paleomagnetic Data. *Geophysical Journal of the Royal Astronomical Society, 62*(3), 699-718 https://doi.org/10.1111/j.1365-246X.1980.tb02601.x

Kissel, C., Laj, C., Rodriguez-Gonzalez, A., Perez-Torrado, F., Carracedo, J. C., & Wandres, C. (2015). Holocene geomagnetic field intensity variations: Contribution from the low latitude Canary Islands site. *Earth and Planetary Science Letters, 430*, 178-190 https://doi.org/10.1016/j.epsl.2015.08.005

Korte, M., & Constable, C. G. (2018). Archeomagnetic Intensity Spikes: Global or Regional Geomagnetic Field Features? *Frontiers in Earth Science, 6* https://doi.org/10.3389/feart.2018.00017

Le Goff, M., & Gallet, Y. (2004). A new three-axis vibrating sample magnetometer for continuous high-temperature magnetization measurements: applications to paleo- and archeo-intensity determinations. *Earth and Planetary Science Letters, 229*(1-2), 31-43 https://doi.org/10.1016/j.epsl.2004.10.025

Lev, R., Bechar, S., & Boaretto, E. (2021). Hazor EB III city abandonment and IBA people return: radiocarbon chronology and its implications. *Radiocarbon, 63*(5), 1453-1469 https://doi.org/10.1017/RDC.2021.76

Levy, T. E., Higham, T., Ramsey, C. B., Smith, N. G., Ben-Yosef, E., Robinson, M., et al. (2008). High-precision radiocarbon dating and historical biblical archaeology in southern Jordan. *Proceedings of the National Academy of Sciences of the United States of America, 105*(43), 16460-16465 https://doi.org/10.1073/pnas.0804950105

Livermore, P. W., Fournier, A., & Gallet, Y. (2014). Core-flow constraints on extreme archeomagnetic intensity changes. *Earth and Planetary Science Letters, 387*, 145-156 https://doi.org/10.1016/j.epsl.2013.11.020

Livermore, P. W., Fournier, A., Gallet, Y., & Bodin, T. (2018). Transdimensional inference of archeomagnetic intensity change. *Geophysical Journal International, 215*(3), 2008-2034 https://doi.org/10.1093/gji/ggy383

Livermore, P. W., Gallet, Y., & Fournier, A. (2021). Archeomagnetic intensity variations during the era of geomagnetic spikes in the Levant. *Physics of the Earth and Planetary Interiors, 312* https://doi.org/10.1016/j.pepi.2021.106657

Masetti-Rouault, M. G. (2016). Assyrian colonization in Eastern Syria: the case of Tell Masaikh (ancient Kar-Ashurnasirpal). In J. MacGinnis, D. Wicke, T. Greenfield, & A. Stone (Eds.), *The provincial archaeology of the Assyrian empire* (pp. 199-212): MacDonald institute monograph.

Martin, M. A. S., Finkelstein, I., & Piasetzky, E. (2020). Radiocarbon-dating the Late Bronze Age: Cultural and historical considerations on Megiddo and beyond. *Bulltin of the American Schools of Oriental Research, 384* https://doi.org/10.1086/709576

Molina-Cardin, A., Campuzano, S. A., Osete, M. L., Rivero-Montero, M., Pavon-Carrasco, F. J., Palencia-Ortas, A., et al. (2018). Updated Iberian Archeomagnetic Catalogue: New Full Vector Paleosecular Variation Curve for the Last Three Millennia. *Geochemistry Geophysics Geosystems, 19*(10), 3637-3656 https://doi.org/10.1029/2018gc007781

Nilsson, A., Holme, R., Korte, M., Suttie, N., & Hill, M. (2014). Reconstructing Holocene geomagnetic field variation: new methods, models and implications. *Geophysical Journal International, 198*(1), 229-248 https://doi.org/10.1093/gji/ggu120

Osete, M. L., Molina-Cardin, A., Campuzano, S. A., Aguilella-Arzo, G., Barrachina-Ibanez, A., Falomir-Granell, F., et al. (2020). Two archaeomagnetic intensity maxima and rapid directional variation rates during the Early Iron Age observed at Iberian coordinates. Implications on the evolution of the Levantine Iron Age Anomaly. *Earth and Planetary Science Letters, 533* https://doi.org/10.1016/j.epsl.2019.116047

Panovska, S., Korte, M., & Constable, C. G. (2019). One hundred thousand years of geomagnetic field evolution. *Reviews of Geophysics, 57*(4), 1289-1337 https://doi.org/10.1029/2019rg000656

Paterson, G. A., Tauxe, L., Biggin, A. J., Shaar, R., & Jonestrask, L. C. (2014). On improving the selection of Thellier-type paleointensity data. *Geochemistry Geophysics Geosystems, 15*(4), 1180-1192 https://doi.org/10.1002/2013gc005135

Pavon-Carrasco, F. J., Osete, M. L., Torta, J. M., & De Santis, A. (2014). A geomagnetic field model for the Holocene based on archaeomagnetic and lava flow data. *Earth and Planetary Science Letters, 388*, 98-109 https://doi.org/10.1016/j.epsl.2013.11.046

Regev, J., Finkelstein, I., Adams, M. J., & E., B. (2014). Wiggled-matched 14C chronology of Early Bronze Megiddo and the synchronization of Egyptian and Levantine chronologies. *Egypt and the Levant 24*, 241-264

Reimer, P. J., Austin, W. E. N., Bard, E., Bayliss, A., Blackwell, P. G., Ramsey, C. B., et al. (2020). The Intcal20 Northern hemisphere radiocarbon age calibration curve (0-55 Cal Kbp). *Radiocarbon, 62*(4), 725-757 https://doi.org/10.1017/Rdc.2020.41

Schanner, M., Korte, M., & Holschneider, M. (2022). ArchKalmag14k: A Kalman-Filter Based Global Geomagnetic Model for the Holocene. *Journal of Geophysical Research-Solid Earth, 127*(2) https://doi.org/10.1029/2021JB023166

Selkin, P. A., & Tauxe, L. (2000). Long-term variations in palaeointensity. *Philosophical Transactions of the Royal Society a-Mathematical Physical and Engineering Sciences, 358*(1768), 1065-1088 https://doi.org/10.1098/rsta.2000.0574

Shaar, R., Bechar, S., Finkelstein, I., Gallet, Y., Martin, M. A. S., Ebert, Y., et al. (2020). Synchronizing Geomagnetic Field Intensity Records in the Levant Between the 23rd and 15th Centuries BCE: Chronological and Methodological Implications. *Geochemistry Geophysics Geosystems, 21*(12) https://doi.org/10.1029/2020GC009251

Shaar, R., Ben-Yosef, E., Ron, H., Tauxe, L., Agnon, A., & Kessel, R. (2011). Geomagnetic field intensity: How high can it get? How fast can it change? Constraints from Iron Age copper slag. *Earth and Planetary Science Letters, 301*(1-2), 297-306 https://doi.org/10.1016/j.epsl.2010.11.013

Shaar, R., Hassul, E., Raphael, K., Ebert, Y., Segal, Y., Eden, I., et al. (2018). The first catalog of archaeomagnetic directions from Israel with 4,000 years of geomagnetic secular variations. *Frontiers in Earth Science, 6* https://doi.org/10.3389/feart.2018.00164

Shaar, R., & Tauxe, L. (2013). Thellier GUI: An integrated tool for analyzing paleointensity data from Thellier-type experiments. *Geochemistry Geophysics Geosystems, 14*(3), 677-692 https://doi.org/10.1002/ggge.20062

Shaar, R., Tauxe, L., Ben-Yosef, E., Kassianidou, V., Lorentzen, B., Feinberg, J. M., & Levy, T. E. (2015). Decadal-scale variations in geomagnetic field intensity from ancient Cypriot slag mounds. *Geochemistry Geophysics Geosystems, 16*(1), 195-214 https://doi.org/10.1002/2014gc005455

Shaar, R., Tauxe, L., Goguitchaichvili, A., Devidze, M., & Licheli, V. (2017). Further evidence of the Levantine Iron Age geomagnetic anomaly from Georgian pottery. *Geophysical Research Letters, 44*(5), 2229-2236 https://doi.org/10.1002/2016gl071494

Shaar, R., Tauxe, L., Ron, H., Ebert, Y., Zuckerman, S., Finkelstein, I., & Agnon, A. (2016). Large geomagnetic field anomalies revealed in Bronze to Iron Age archeomagnetic data from Tel Megiddo and Tel Hazor, Israel. *Earth and Planetary Science Letters, 442*, 173-185 https://doi.org/10.1016/j.epsl.2016.02.038

Tauxe, L., Banerjee, S. K., Butler, R. F., & Van der Voo, R. (2018). *Essentials of Paleomagnetism* (5th Web ed.).

Tauxe, L., Shaar, R., Jonestrask, L., Swanson-Hysell, N. L., Minnett, R., Koppers, A. A. P., et al. (2016). PmagPy: Software package for paleomagnetic data analysis and a bridge to the Magnetics Information Consortium (MagIC) Database. *Geochemistry Geophysics Geosystems, 17*(6), 2450-2463 https://doi.org/10.1002/2016gc006307

Tauxe, L., & Staudigel, H. (2004). Strength of the geomagnetic field in the Cretaceous Normal Superchron: New data from submarine basaltic glass of the Troodos Ophiolite. *Geochemistry Geophysics Geosystems, 5* https://doi.org/10.1029/2003GC000635

Toffolo, M. B., Arie, E., Martin, M. A. S., Boaretto, E., & Finkelstein, I. (2014). Absolute chronology of Megiddo, Israel, in the Late Bronze and Iron Ages: High-resolution radiocarbon dating. *Radiocarbon, 56*(1), 221-244 https://doi.org/10.2458/56.16899

Troyano, M., Fournier, A., Gallet, Y., & Finlay, C. C. (2020). Imprint of magnetic flux expulsion at the core-mantle boundary on geomagnetic field intensity variations. *Geophysical Journal International, 221*(3), 1984-2009 https://doi.org/10.1093/gji/ggaa126

Vaknin, Y., Shaar, R., Gadot, Y., Shalev, Y., Lipschits, O., & Ben-Yosef, E. (2020). The Earth's magnetic field in Jerusalem during the Babylonian destruction: A unique reference for field behavior and an anchor for archaeomagnetic dating. *Plos One, 15*(8) https://doi.org/10.1371/journal.pone.0237029

Vaknin, Y., Shaar, R., Lipschits, O., Mazar, A., Maeir, A., Garfinkel, Y., et al. (submitted). Reconstructing biblical military campaigns using geomagnetic field data *Nature Communications*

Yu, Y. J., Tauxe, L., & Genevey, A. (2004). Toward an optimal geomagnetic field intensity determination technique. *Geochemistry Geophysics Geosystems, 5* https://doi.org/10.1029/2003gc000630